Models of the Low-Spin Iron(III) Hydroperoxide Intermediate of Heme Oxygenase: Magnetic Resonance Evidence for Thermodynamic Stabilization of the d x y Electronic State at Ambient...

ARTICLE *in* JOURNAL OF THE AMERICAN CHEMICAL SOCIETY · MAY 2002

Impact Factor: 12.11 · DOI: 10.1021/ja017334o

J|A|C|S
ARTICLES
Published on Web 04/24/2002

Models of the Low-Spin Iron(III) Hydroperoxide Intermediate of Heme Oxygenase: Magnetic Resonance Evidence for Thermodynamic Stabilization of the d_{xy} Electronic State at Ambient Temperatures

Mario Rivera,*,† Gregori A. Caignan,† Andrei V. Astashkin,*,‡ Arnold M. Raitsimring,‡ Tatjana Kh. Shokhireva,‡ and F. Ann Walker*,‡

Contribution from the Department of Chemistry, Oklahoma State University, Stillwater, Oklahoma 74078-3071, and Department of Chemistry, University of Arizona, Tucson, Arizona 85721-0041

Received October 19, 2001

Abstract: The ^{13}C pulsed ENDOR and NMR study of [*meso*-^{13}C-TPPFe(OCH_3)(OO^tBu)]$^-$ performed in this work shows that although the unpaired electron in low-spin ferrihemes containing a ROO^- ligand resides in a d_π orbital at 8 K, the d_{xy} electron configuration is favored at physiological temperatures. The variable temperature NMR spectra indicate a dynamic situation in which a heme with a d_π electron configuration and planar porphyrinate ring is in equilibrium with a d_{xy} electron configuration that has a ruffled porphyrin ring. Because of the similarity in the EPR spectra of the hydroperoxide complexes of heme oxygenase, cytochrome P450, and the model heme complex reported herein, it is possible that these two electron configurations and ring conformations may also exist in equilibrium in the enzymatic systems. The ruffled porphyrinate ring would aid the attack of the terminal oxygen of the hydroperoxide intermediate of heme oxygenase (HO) on the *meso*-carbon, and the large spin density at the *meso*-carbons of a d_{xy} electron configuration heme suggests the possibility of a radical mechanism for HO. The dynamic equilibrium between the ruffled (d_{xy}) and planar (d_π) conformers observed in the model complexes also suggests that a flexible heme binding cavity may be an important structural motif for heme oxygenase activity.

Introduction

The degradation of heme in mammalian cells is catalyzed by the enzyme heme oxygenase (HO).[1−3] In a molecular oxygen- and electron-dependent set of reactions, HO cleaves the α-*meso* bridge of protohemin to produce CO, biliverdin, and free iron. Not long ago, the HO system was regarded only in the context of the maintenance of cellular heme homeostasis as a catabolic enzyme, and the products of HO activity were considered toxic waste material. More recently, this view has changed drastically after the discovery that all products of HO enzymatic action possess important biological activity. CO functions to regulate vasomotor tone and neurotransmission in a manner akin to NO,[4,5] iron released from HO activity upregulates ferritin expression,[6] and bilirubin, formed when biliverdin is reduced by biliverdin reductase, is a potent antioxidant.[7] Because the regulation of HO activity has ramifications for a variety of physiological functions, it is important to attain a detailed understanding of the mechanism by which heme is converted to CO, Fe, and biliverdin.

Although several important aspects of the mechanism of action of HO have not yet been elucidated, the evidence gathered so far demonstrates that HO acts via a mechanism different from that currently accepted for other oxygen activating hemoproteins such as cytochromes P450, peroxidases, and catalases (recently reviewed),[1−3,8] as well as the mitochondrial enzyme complex, cytochrome *c* oxidase (recently reviewed).[9] Nevertheless, the reactions catalyzed by HO display some of the characteristic fundamental aspects shared by the catalytic mechanism of action of all oxygen-activating heme proteins. The ferric enzyme is initially reduced to its ferrous state,[10] followed by formation of an oxyferrous complex (Fe^{II}-O_2), which accepts a second electron from NADPH cytochrome P450 reductase, and thereby is transformed into a ferric hydroperoxy (Fe^{III}-OOH) species.[10] On the basis of the reactivity of HO toward hydrogen peroxide and alkyl hydroperoxides, it was proposed that the nature of the species that oxidizes the HO-bound heme to α-*meso*-hydroxyheme is a ferric hydroperoxide (Fe^{III}-OOH).[3,10] Strong evidence supporting this conclusion was recently produced by cryo-

* To whom correspondence should be addressed. E-mail: Rivera@okstate.edu.
† Oklahoma State University.
‡ University of Arizona.

(1) Ortiz de Montellano, P. R. *Acc. Chem. Res.* **1998**, *31*, 543−549.
(2) Ortiz de Montellano, P. R. *Curr. Opin. Chem. Biol.* **2000**, *4*, 221−227.
(3) Ortiz de Montellano, P. R.; Wilks, A. *Adv. Inorg. Chem.* **2000**, *51*, 359−407.
(4) Stupfel, M.; Bouley, G. *Ann. N.Y. Acad. Sci.* **1970**, *174*, 342.
(5) Morita, T.; Kourembanas, S. *J. Clin. Invest.* **1995**, *96*, 2676−2682.
(6) Einstein, R. S.; Garcia-Mayo, D.; Pettingell, W.; Munroe, H. N. *Proc. Natl. Acad. Sci. U.S.A.* **1991**, *88*, 688−692.
(7) Stocker, R.; Yamamoto, Y.; McDonagh, A. F.; Glazer, A. N.; Ames, B. N. *Science* **1987**, *235*, 1043−1046.
(8) Loew, G. H. *Chem. Rev.* **2000**, *100*, 407−419.
(9) Sucheta, A.; Georgiadis, K. E.; Einarsdottir, O. *Biochemistry* **1997**, *36*, 554−565.
(10) Wilks, A.; Torpey, J.; Ortiz de Montellano, P. R. *J. Biol. Chem.* **1994**, *269*, 29553−29556.

reduction of the ferrous dioxygen complex of HO (Fe^{II}-O_2) to produce an intermediate that was identified by EPR spectroscopy as corresponding to the Fe^{III}-OOH complex.[11] Upon warming, this intermediate was converted into the corresponding α-*meso*-hydroxyheme complex, thus confirming a ferric hydroperoxide intermediate as a precursor of α-*meso*-hydroxyheme.

The EPR spectrum corresponding to the Fe^{III}-OOH complex of HO displays *g*-values of 2.37 (or 2.38, depending on treatment), 2.19, and 1.93 at 77 K.[11] The sum of the squares of the principal *g*-values ($\sum g^2$) for the hydroperoxy complex of HO is about 14.1. It is interesting to consider this value in the context of recently reported studies of low-spin Fe(III) porphyrinates.[12−15] These reports demonstrated the presence of a novel electronic configuration, $(d_{xz},d_{yz})^4(d_{xy})^1$, where the unpaired electron resides in the d_{xy} orbital. Interestingly, all model hemes known to possess the $(d_{xz},d_{yz})^4(d_{xy})^1$ electron configuration (hereafter abbreviated as d_{xy}) displayed EPR spectra with $\sum g^2 < 14$. By comparison, low-spin Fe(III) hemes possessing the more common $(d_{xy})^2(d_{xz},d_{yz})^3$ electron configuration (hereafter abbreviated as d_π) display EPR spectra with the typical $g_{xx}^2 + g_{yy}^2 + g_{zz}^2 \approx 16$.[14,16]

On the basis of these arguments, it was possible to speculate that the electronic configuration of the Fe^{III}-OOH complex of HO might have an unpaired electron residing in the d_{xy} orbital. What is noteworthy about a d_{xy} electronic configuration is that it places a large amount of π-spin density on the porphyrin *meso*-carbons.[12−16] To delocalize spin density from the d_{xy} orbital into the porphyrin π system, the macrocycle has to ruffle significantly, so that the nodal planes of the p_z orbitals of the macrocycle are no longer in the *xy* plane; the components (projections) of these p_z orbitals in the *xy* plane have the proper symmetry to interact with the d_{xy} orbital.[12] The porphyrin orbital that has the proper symmetry to interact with the d_{xy} orbital in this ruffled macrocycle conformation is the $3a_{2u}(\pi)$ orbital[12] shown in Figure 1. It is evident from the relative sizes of the circles in the schematic representation of the $3a_{2u}(\pi)$ orbital that the *meso*-carbons possess large electron density. Large spin density at the meso positions, in turn, may explain the attack of the Fe^{III}-OOH intermediate on a heme *meso*-carbon, as discussed in more detail later in this work. Consequently, the main object of the investigations reported herein is to determine the electron configuration of hydroperoxide or alkyl peroxide complexes of Fe^{III} porphyrinates.

Some years ago Tajima and co-workers showed that synthetic hemes in the presence of alkyl peroxides and a variety of sixth ligands, including methoxide,[17−19] imidazolate,[20] or a second alkyl peroxide,[19] as well as heme proteins with histidine[21,22] or cysteinate[23] sixth ligands, yield very similar EPR spectra with compressed *g* anisotropy ($\sum g^2 \approx 14$). These spectra are very similar to those obtained for the Fe^{III}-OOH complexes of various heme protein enzymes, which were prepared by cryoreduction and then annealing of the corresponding Fe^{II}-O_2 complexes.[11,24] The *g*-values of the complexes of Tajima and co-workers (2.32, 2.16, 1.95, methoxide, *tert*-butylperoxide;[21] 2.25, 2.15, 1.96, bis-*tert*-butyl-peroxide;[21] 2.32, 2.19, 1.94, imidazolate, hydroperoxide[20]) are very similar to those of annealed hemoglobin-hydroperoxide (2.31, 2.18, 1.94),[11] heme oxygenase-hydroperoxide (2.37, 2.19, 1.93),[11] and cytochrome P450-hydroperoxide (2.29, 2.16, 1.96).[24] We thus reasoned that magnetic resonance investigation of the Tajima model complexes could provide important information concerning the orbital of the unpaired electron, and hence the likely conformation of the porphyrinate ring of these model complexes, which could thus yield insights into the electronic and molecular structure of the catalytically active hydroperoxide complex of heme oxygenase. As will be shown below, we find that at 8 K the unpaired electron of $[TPPFe(OCH_3)(OO^tBu)]^-$, $[TPPFe(OO^tBu)_2]^-$, and $[TPPFe(OCH_3)_2]^-$ resides in one of the d_π orbitals, while at physiological temperatures the unpaired electron of those complexes that are stable enough to investigate is indeed in the d_{xy} orbital.

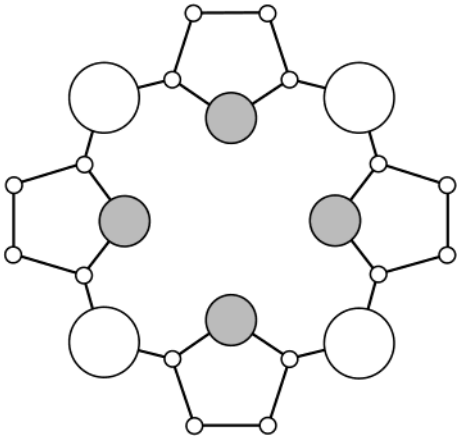

Figure 1. Representation of the $3a_{2u}(\pi)$ porphyrin orbital. The sizes of the circles are proportional to the calculated electron density.

Experimental Section

Reagents. Tetramethylammonium hydroxide (TMAOH) 25% (w/w) in methanol and 70% (w/w) aqueous *tert*-butylhydroperoxide (^{t}BuOOH) were purchased from Alfa Aesar. TMAOH was used as received, whereas ^{t}BuOOH was extracted into methylene chloride by swirling 2.5 mL of the aqueous peroxide solution with 6 mL of dichloromethane in a separatory funnel. The organic phase was separated and then dried over anhydrous $MgSO_4$ before being filtered into a brown glass container. Dichloromethane solutions of ^{t}BuOOH were prepared before each experiment. Chloroiron(III) tetraphenylporphyrin (TPPFeCl) and *meso*-^{13}C-TPPFe^{III}Cl were purchased from Porphyrin Products (Logan, UT) and used without further purification. ^{13}C labeled perchlorato-

(11) Davydov, R. M.; Yoshida, T.; Ikeda-Saito, M.; Hoffman, B. M. *J. Am. Chem. Soc.* **1999**, *121*, 10656−10657.
(12) Safo, M. K.; Walker, F. A.; Raitsimring, A. M.; Walters, W. P.; Dolata, D. P.; Debrunner, P. G.; Scheidt, W. R. *J. Am. Chem. Soc.* **1994**, *116*, 7760−7770.
(13) Walker, F. A.; Nasri, H.; Torowska-Tyrk, I.; Mohanrao, K.; Watson, C. T.; Shkhirev, N. V.; Debrunner, P. G.; Scheidt, W. R. *J. Am. Chem. Soc.* **1996**, *118*, 12109−12118.
(14) Walker, F. A. *Coord. Chem. Rev.* **1999**, *185*−*186*, 471−534.
(15) Simonneaux, G.; Schünemann, V.; Morice, C.; Carel, L.; Toupet, L.; Winkler, H.; Trautwein, A. X.; Walker, F. A. *J. Am. Chem. Soc.* **2000**, *122*, 4366−4377.
(16) Walker, F. A. Proton NMR and EPR Spectroscopy of Paramagnetic Metalloporphyrins. In *The Porphyrin Handbook*; Kadish, K. M., Smith, K. M., Guilard, R., Eds.; Academic Press: San Diego, 2000; pp 81−183.
(17) Tajima, K.; Ishizu, K.; Sakurai, H.; Nishiguchi-Ohya, H. *Biochem. Biophys. Res. Commun.* **1986**, *135*, 972−978.
(18) Tajima, K.; Jinno, J.; Ishizu, K.; Sakurai, H.; Ohya-Nishiguchi, H. *Inorg. Chem.* **1989**, *28*, 709−715.
(19) Tajima, K.; Tada, K.; Jinno, J.; Edo, T.; Mano, H.; Azuma, N.; Makino, K. *Inorg. Chim. Acta* **1997**, *254*, 29−35.
(20) Tajima, K.; Oka, S.; Edo, T.; Miyake, S.; Mano, H.; Mukai, K.; Sakurai, H.; Ishizu, K. *J. Chem. Soc., Chem. Commun.* **1995**, 1507−1508.
(21) Tajima, K. *Inorg. Chim. Acta* **1990**, *169*, 211−219.
(22) Jinno, J.; Shigematsu, M.; Tajima, K.; Sakurai, H.; Ohya-Nishiguchi, H.; Ishizu, K. *Biochem. Biophys. Res. Commun.* **1991**, *176*, 675−681.
(23) Tajima, K.; Edo, T.; Ishizu, K.; Imaoka, S.; Funae, Y.; Oka, S.; Sakurai, H. *Biochem. Biophys. Res. Commun.* **1993**, *191*, 157−164.
(24) Davydov, R.; Macdonald, I. D. G.; Makris, T. M.; Sligar, S. G.; Hoffman, B. M. *J. Am. Chem. Soc.* **1999**, *121*, 10654−10655.

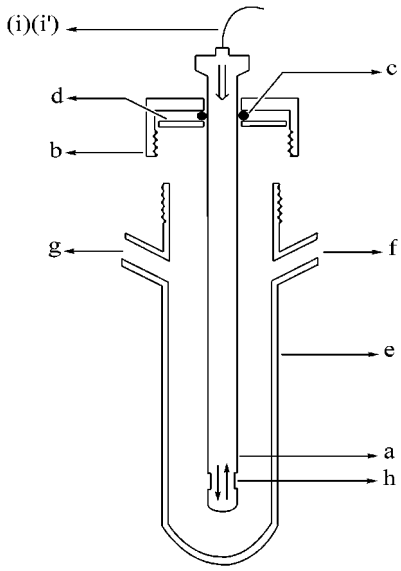

Figure 2. Schematic cross-sectional representation of the cell used to obtain electronic absorption spectra at low temperatures: (a) dip probe, (b) threaded cell-cap, (c) O-ring; when the cap is threaded into position, the teflon washer (d) forces the O-ring to expand, thus producing an airtight seal. The cell body is outfitted with a port for argon inlet (f) and a port for reagent delivery and argon outlet (g). The latter can be sealed with a rubber septum. The sampling cavity (h) utilized in the experiments has a path length of 0.2 cm, and the dip probe is connected to the excitation source and diode array detector via optical fibers (i).

iron(III) tetraphenylporphyrin (*meso*-^{13}C-TPPClO$_4$) was prepared from *meso*-TPPFeCl according to a published procedure.[25]

Synthesis of Alkyl Peroxide Porphyrinate Complexes. Alkyl peroxide complexes of TPPFe were synthesized by a modification of the synthetic procedures reported by Tajima and co-workers.[17−23] These investigators reported the synthesis and characterization (EPR and electronic absorption spectra) of [FeTPP(OCH$_3$)$_2$]$^-$, [TPPFe(OCH$_3$)(OO^{t}Bu)]$^-$, and [TPPFe(OO^{t}Bu)$_2$]$^-$ in frozen glasses at 77 K. An important aim of the investigations reported here is the study of these complexes by ^{13}C NMR spectroscopy in solution. Consequently, modifications were necessary to synthesize and characterize the complexes at temperatures above the melting point of CH_2Cl_2. As a first step toward this goal, conditions were explored that allowed us to reproduce the electronic absorption spectra, previously obtained from frozen glasses at 77 K,[17−19] in solutions thermostated at 195 K. To facilitate these experiments, the cell shown in Figure 2 was constructed out of glass. To assemble the cell, the "dip probe" (a) is inserted through the cap (b) and secured with the O-ring (c) and teflon washer (d). The cap is then threaded onto the main body of the cell (e), where it will push upon the washer, causing the O-ring to expand, thereby making the assembly gastight. Two side-ports were built into the glass cell: the first (f) serves as an inlet for argon, needed to establish a water-free atmosphere; the second (g) is fitted with a rubber septum, which can be removed for the addition of reactants. Reagents are introduced into the cell with the aid of polyethylene capillary tubing (0.8 mm i.d., 1.8 mm o.d.) and a peristaltic pump. The dip probe (Ocean Optics, Dunedin, FL) enables ultraviolet and visible light from the excitation source to be directed into the sample solution through a fiber optic (i). The light passes through the solution in the probe cavity (h) and is reflected by a mirror back to a second fiber optic (i′), to be sent to a detector (Ocean Optics, UV−vis S2000) where the signal is processed. The probe can be equipped with sampling cavities of varying path lengths. For the purposes of these studies, a sampling cavity with a 0.2 cm path length was used.

(25) Nesset, M. J. M.; Cai, S.; Shokhireva, T. Kh.; Shokhirev, N. V.; Jacobson, S. E.; Jayaraj, K.; Gold, A.; Walker, F. A. *Inorg. Chem.* **2000**, *39*, 532−540.

A typical procedure for synthesizing the alkyl peroxide complexes is described in what follows: A dichloromethane solution of TPPFeCl (6 mL, 0.2 mM), previously dried over MgSO$_4$, was added into the cell through the reagent port (g). The cell was then thermostated at −78 °C with the aid of an acetone-dry ice bath. It is important to maintain a constant stream of argon to avoid the condensation of atmospheric water inside the cell. A solution of TMAOH in methanol (100 μL, 2.4 M) was added to the solution containing TPPFeCl, thus generating [TPPFe(OCH$_3$)$_2$]$^-$. The resultant solution was frozen by immersing the cell in liquid nitrogen, followed by the addition of a solution of ^{t}BuOOH in CH_2Cl_2 (125 μL, 1 M). The latter freezes almost instantaneously on the surface of the frozen solution of [TPPFe(OCH$_3$)$_2$]$^-$. The cell is then transferred back to an acetone-dry ice bath, where the solid solution is allowed to thaw at −78 °C with continuous stirring. The color of the solution changes to a cherry red. The electronic absorption spectrum recorded at −78 °C in this "dip probe" cell is very similar to that reported for [TPPFe(OCH$_3$)(OO^{t}Bu)]$^-$ at 77 K.[19] Similar experiments allowed us to determine that the molar proportions needed to obtain electronic absorption spectra characteristic of the different alkyl peroxide complexes at −78 °C are 1 TPPFeCl (0.2 mM):200 OH$^-$:100 ^{t}BuOOH for [TPPFe(OCH$_3$)(OO^{t}Bu)]$^-$, and 1 TPPFeCl (0.2 mM):200 OH$^-$:600 ^{t}BuOOH for [TPPFe(OO^{t}Bu)$_2$]$^-$. These proportions were subsequently utilized to synthesize the complexes for magnetic resonance spectroscopic studies.

Sample Preparation for Magnetic Resonance Spectroscopic Studies. The alkyl peroxide complexes were synthesized at −78 °C in an EPR or NMR tube. A typical synthesis was carried out as follows: The NMR/EPR tube is flushed with argon through a polyethylene capillary tube. A solution of *meso*-^{13}C-TPPFeCl (500 μL, 3 mM) in CD_2Cl_2 was added into an NMR/EPR tube with the aid of a second polyethylene capillary tube and a peristaltic pump. TMAOH (125 μL, 2.4 M) is then introduced into the NMR/EPR tube in a similar fashion, thus resulting in the formation of [*meso*-^{13}C-TPPFe(OCH$_3$)$_2$]$^-$. Mixing of the solutions was performed with the help of a thin (∼1 mm diameter) ceramic rod. The ceramic rod was left in the solution and the NMR tube immersed in liquid nitrogen, while constantly flushing with a stream of argon. To synthesize [*meso*-^{13}C-TPPFe(OCH$_3$)(OO^{t}Bu)]$^-$, a solution of ^{t}BuOOH (50 μL, 3 M) was then carefully added with the aid of a clean polyethylene capillary tube and a peristaltic pump. The solution of ^{t}BuOOH freezes almost instantaneously on top of the frozen solution of [*meso*-^{13}C-TPPFe(OCH$_3$)$_2$]$^-$. The NMR/EPR tube is then transferred to an acetone-dry ice bath and the solutions allowed to melt while mixing with the ceramic rod. The tube is capped, and the solution containing the alkyl peroxide complex is frozen in liquid nitrogen and transferred into a previously thermostated NMR probe or EPR cavity. TPPFe(OCH$_3$) for ^{1}H NMR experiments was prepared by addition of 2 μL of a freshly prepared solution of NaOCH$_3$ (∼2.4 M) to 500 μL of 3 mM TPPFeClO$_4$ in toluene-d_8. The synthesis was carried out at room temperature, in an NMR tube, as described above. The mono-methoxy complex used in the electronic absorption experiments was prepared in the anaerobic cell described above. In short, 2 μL of NaOCH$_3$ (2.4 M) was added to 500 μL of a 3 mM solution of TPPFeClO$_4$ in toluene, a solvent that does not support ionic species, hence stabilizing the mono-methoxy complex.

NMR Spectroscopic Investigations. ^{13}C NMR spectra of [*meso*-^{13}C-TPPFe(OCH$_3$)(OO^{t}Bu)]$^-$ were obtained on a Varian Unity Inova spectrometer operating at a ^{13}C frequency of 100.576 MHz. The spectra were acquired over 16 k data points, with a spectral width of 8.6 kHz, 90 ms acquisition time, 40 ms relaxation delay, and 40 000 scans. The baseline was flattened with a spline fitting of predefined baseline regions. The temperature of the sample was set and regulated through the use of a standard variable temperature unit furnished by Varian Instruments, which functions by controlling a heating element which is exposed to a stream of cooled gas. The variable temperature unit was calibrated by using the Wilmad temperature calibration sample,

which utilizes the temperature-dependent difference in resonance frequency of the two peaks of methanol.

EPR Spectroscopic Investigations. Continuous wave EPR spectra were recorded on a Bruker ESP-300E spectrometer, at 77 K, using an immersion dewar. The pulsed ENDOR experiments were carried out on the home-built X/P-band pulsed EPR spectrometer[26] equipped with a pulsed ENDOR accessory.[27] In these experiments, the Mims[28] and Davies[29] pulsed ENDOR techniques were employed. To minimize the Mims ENDOR spectrum distortions due to the blind spots,[30,31] the spectra were detected at several time intervals τ between the first and second microwave (mw) pulses of the three-pulse sequence, and then summed. The measurement temperature, chosen to optimize the electron spin relaxation times for the pulsed EPR experiments, was about 8 K.

Results and Discussion

Synthesis of Alkyl Peroxide Complexes of Fe^{III}TPP. Tajima and co-workers have described the synthesis of alkyl peroxide complexes of Fe^{III}-tetraphenylporphyrin, such as $[TPPFe(OCH_3)_2]^-$, $[TPPFe(OCH_3)(OO^tBu)]^-$, and $[TPPFe(OO^tBu)_2]^-$, in several reports.[17−23] Three important aspects prompted us to reinvestigate the synthesis of alkyl peroxide complexes previously reported by Tajima et al.: (a) The stoichiometric proportions needed to prepare the alkyl peroxide complexes are significantly different from one report to another. In our hands, the stoichiometric proportions previously reported do not lead to the synthesis of the desired alkyl peroxide complexes. (b) The alkyl peroxide (^{t}BuOOH), utilized in the previous reports, was distilled under reduced pressure, a step that is potentially hazardous, and at best could lead to significant decomposition of the peroxide. We have thus used aqueous ^{t}BuOOH extracted into CH_2Cl_2, followed by drying with $MgSO_4$. (c) The alkyl peroxide complexes prepared by Tajima et al. have been studied only in frozen glasses at 77 K.[17−23] Because it was our intention to conduct ^{13}C NMR spectroscopic studies of the alkyl peroxide complexes in solution, it was important to search for appropriate conditions for the preparation of the complexes at temperatures above the melting point of CH_2Cl_2. Consequently, the alkyl peroxide complexes were prepared at −78 °C (195 K), and the formation of products was monitored with the aid of electronic absorption spectroscopy. The appropriate stoichiometric proportions needed to prepare $[TPPFe(OCH_3)(OO^tBu)]^-$ were determined by comparing the electronic absorption spectrum obtained in solution at 195 K with those reported by Tajima et al. in frozen glasses at 77 K.[17−19] To ensure that the conditions found by electronic absorption spectroscopy could be more readily translated into the concentrations needed for the NMR and EPR spectroscopic experiments, the "dip probe" (see Experimental Section) was outfitted with a 2.0 mm path cavity, and only the visible region (450−800 nm) of the spectrum was monitored. This allowed us to increase the concentration of porphyrin severalfold relative to what is possible if one utilizes an optical path of 1 cm and observes the Soret band. In fact, the concentration used to prepare the alkyl peroxide complexes for the NMR experiments is only 4-fold higher than that used with the electronic absorption spectroscopy studies. This increased concentration should maintain the thermodynamic stability of the complex, even in the face of increased temperature (178−218 K), by overcoming the expected decrease in K_{eq} for complex formation as the temperature is raised. Experiments conducted in this fashion allowed us to establish that the addition of a 200-fold molar excess of tetramethylammonium hydroxide in methanol to a solution containing TPPFeCl in CH_2Cl_2 results in the formation of a complex that displays the electronic spectrum shown in Figure 3A. When the complex is prepared in an EPR tube (see Experimental Section) and the resultant solution is frozen at 77 K for spectroscopic analysis, an EPR spectrum (Figure 3D, trace 1) identical to that reported by Tajima et al.[18,19] for $[TPPFe(OCH_3)_2]^-$ is obtained. The addition of a 100-fold excess of ^{t}BuOOH, with respect to TPPFeCl, to $[TPPFe(OCH_3)_2]^-$ results in the formation of $[TPPFe(OCH_3)(OO^tBu)]^-$. The electronic absorption spectrum of this complex at 195 K (Figure 3B) and EPR spectrum at 77 K (Figure 3D, trace 2) are characteristic of a low-spin iron(III) porphyrinate and very similar to those reported for $[TPPFe(OCH_3)(OO^tBu)]^-$ at 77 K.[18,19] NMR spectroscopic analysis of the organic layer obtained after extracting aqueous ^{t}BuOOH into CD_2Cl_2 indicated that there is a small amount of ^{t}BuOH present (∼5%). Hence, it was important to eliminate the possibility that coordination of ^{t}BuOH may form $[TPPFe(OCH_3)(O^tBu)]^-$ or $[TPPFe(O^tBu)_2]^-$ as the species giving rise to the electronic and EPR spectra shown in Figure 3B and D, trace 2. To this end, an experiment was conducted in which ^{t}BuOH (200-fold excess with respect to TPPFeCl) was added to $[TPPFe(OCH_3)_2]^-$. The addition of ^{t}BuOH did not bring any changes to the spectrum of [TPPFe-

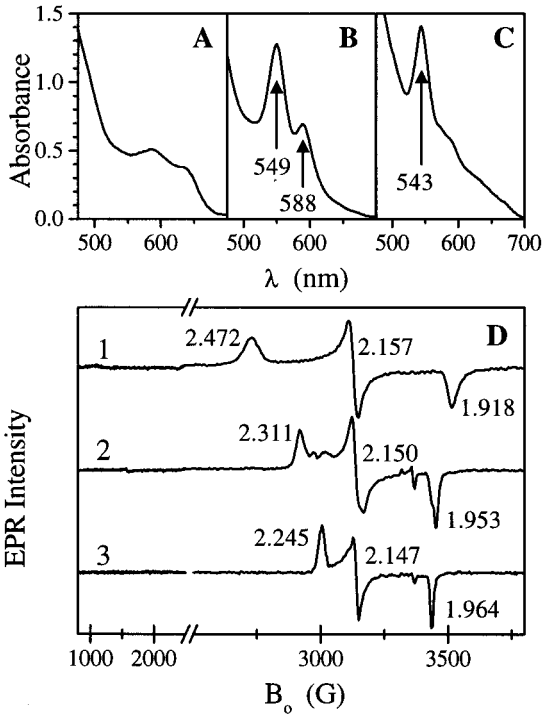

Figure 3. Electronic absorption spectra of $[TPPFe(OCH_3)_2]^-$ (A), $[TPPFe(OCH_3)(OO^tBu)]^-$ (B), and $[TPPFe(OO^tBu)_2]^-$ (C). The corresponding EPR spectra are shown in (D) by traces 1, 2, and 3, respectively. The small peaks at $g = 2$ in traces 2 and 3 are due to ^{t}BuOO•.

(26) Borbat, P. P.; Raitsimring, A. M. *Abstracts of 36th Rocky Mountain Conference on Analytical Chemistry*; Denver, CO, July 31−August 5, 1994; p 94.
(27) Astashkin, A. V.; Mader Cosper, M.; Raitsimring, A. M.; Enemark, J. H. *Inorg. Chem.* **2000**, *39*, 4989−4992.
(28) Mims, W. B. *Proc. R. Soc. London* **1965**, *283*, 482−457.
(29) Davies, E. R. *Phys. Lett. A* **1974**, *47*, 1−2.
(30) Grupp, A.; Mehring, M. Pulsed ENDOR Spectroscopy in Solids. In *Modern Pulsed and Continuous Wave Electron Spin Resonance*; Kevan, L., Bowman, M., Eds.; Wiley: New York, 1990; pp 195−229.
(31) Thomann, H.; Bernardo, M. Pulsed Electron Nuclear Multiple Resonance Spectroscopic Methods for Metalloproteins and Metalloenzymes. In *Methods in Enzymology*; Riordan, J. F., Vallee, B. L., Eds.; Academic Press: San Diego, 1993; Vol. 227, pp 118−189.

$(OCH_3)_2]^-$, thus clearly demonstrating that the electronic and EPR spectra shown in Figure 3B and D, trace 2, correspond to $[TPPFe(OCH_3)(OO^tBu)]^-$ and not $[TPPFe(OCH_3)(O^tBu)]^-$. Addition of more ^{t}BuOOH to a solution of $[TPPFe(OCH_3)(OO^tBu)]^-$, 600-fold excess with respect to TPPFeCl, results in the formation of $[TPPFe(OO^tBu)_2]^-$. The EPR spectrum of this complex at 77 K (Figure 3D, trace 3) is identical to that reported by Tajima and co-workers[18,19] for $[TPPFe(OO^tBu)_2]^-$. It can also be seen from Figure 3C that the electronic spectrum of $[TPPFe(OO^tBu)_2]^-$ at 178 K is characteristic of a low-spin porphyrinate, and clearly distinct from the electronic spectrum exhibited by $[TPPFe(OCH_3)(OO^tBu)]^-$. The electronic spectrum of $[TPPFe(OO^tBu)_2]^-$ had not been reported previously.

The results summarized above clearly indicate that the stoichiometric proportions of reactants utilized to synthesize the different alkyl peroxide complexes at 195 K produce solutions with optical signatures very similar to those obtained by Tajima et al. at 77 K.[18−20] In addition, EPR spectra of the low-spin complexes synthesized with these stoichiometric proportions are not only identical to those reported previously,[18−20] but also do not contain the high-spin Fe(III) EPR signals, present in some of the previous reports.[17,18,20,21] Consequently, it can be concluded that the alkyl peroxide complexes, previously characterized only at 77 K,[17−21] are also stable at 195 K. A second point of practical importance in the synthesis of these alkyl peroxide complexes is that it is not necessary to distill the alkyl hydroperoxide. It is sufficient to extract ^{t}BuOOH from its aqueous commercial solution into CH_2Cl_2, followed by drying the organic phase with $MgSO_4$. The CH_2Cl_2 solution of ^{t}BuOOH obtained in this manner permits the successful synthesis of the alkyl peroxide complexes at 195 K if care is taken to exclude atmospheric water from the system.

Pulsed ENDOR Spectroscopy Reveals that $[TPPFe(OCH_3)(OO^tBu)]^-$ Has a d_π Electron Configuration at 8 K. It is evident from the EPR spectra summarized in Figure 3 that $\sum g^2 \leq 14$ for $[TPPFe(OCH_3)(OO^tBu)]^-$ and $[TPPFe(OO^tBu)_2]^-$. This raised the possibility that these complexes might possess a d_{xy} electron configuration. This possibility was investigated by pulsed ENDOR at 8 K and by ^{13}C NMR spectroscopy at higher temperatures (see below). The Mims ENDOR[27] spectra of [*meso*-^{13}C-$TPPFe(OCH_3)(OO^tBu)]^-$, recorded at the low-field (g_{LF}) and high-field (g_{HF}) extrema of the EPR spectrum, are shown in Figure 4, traces 1 and 2. Traces 3 and 4 in the same figure show the spectra of [*meso*-^{13}C-$TPPFe(N\text{-}MeIm)_2]^+$, an example of a "pure" d_π electron configuration.[13−16] The hyperfine splittings in all spectra do not exceed 1.7 MHz. In the ENDOR spectra recorded at the intermediate positions of the EPR spectra, the splittings are similar (not shown).

Figure 5 shows for comparison the pulsed ENDOR spectra of [*meso*-^{13}C-$TPPFe(^tBuNC)_2]^+$, an example of a "pure" d_{xy} electron configuration,[14,16] recorded at $g_{LF} = g_X = g_Y$ (trace 1), $g_{HF} = g_Z$ (trace 5), and at intermediate g-values that correspond to different angles θ_{BZ} between the external magnetic field $\mathbf{B_0}$ and the normal $\mathbf{Z}$ to the heme plane (at g_{LF}, $\theta_{BZ} = 90°$, and at g_{HF}, $\theta_{BZ} = 0°$, as indicated in Figure 5). The spectra in Figures 4 and 5 are considerably different both in appearance and in the frequencies of the ^{13}C transitions, and can be used "as is" to distinguish one electronic configuration from the other. Thus, we can already make a conclusion that the ENDOR spectra clearly indicate that at 8 K the electron

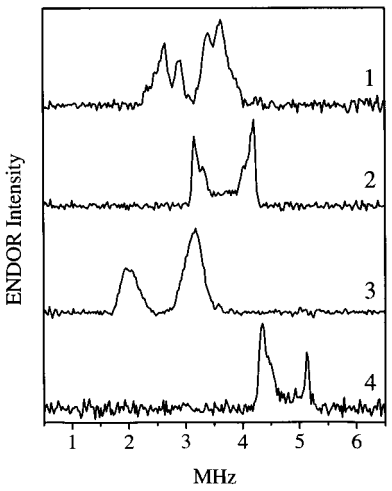

Figure 4. Mims ENDOR spectra of *meso*-^{13}C in $[TPPFe(OCH_3)(OO^tBu)]^-$ (traces 1 and 2) and in $[TPPFe(N\text{-}MeIm)_2]^+$ (traces 3 and 4). The spectra were obtained as differences between those of the samples enriched with ^{13}C and the samples with a natural abundance of isotopes (∼1% of ^{13}C). Traces 1 and 2 are detected at $B_o = 2920$ G ($g_{LF} = g_Z$) and $B_o = 3430$ G ($g_{HF} = g_X$), respectively. They represent a result of summation of spectra recorded at the time intervals τ between the first and second microwave (mw) pulses of 300, 400, 500, and 600 ns. Traces 3 and 4 are detected at $B_o = 2385$ G ($g_{LF} = g_Z$) and $B_o = 4425$ G ($g_{HF} = g_X$), respectively. Trace 3 represents a result of summation of the spectra obtained at $\tau = 250$, 350, 450, and 550 ns, while trace 4 is a result of summation of the spectra at $\tau = 250$ and 350 ns. Experimental conditions: temperature, ∼8 K; mw frequency, 9.445 GHz; time interval T between the second and third mw pulses, 60 μs; radio frequency pulse duration, $T_{RF} = 30$ μs (about 180° for weakly coupled ^{13}C).

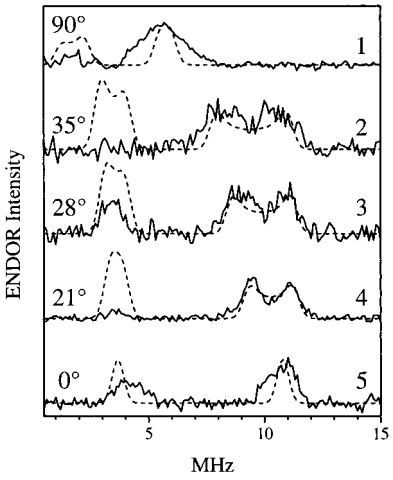

Figure 5. Davies ENDOR spectra of *meso*-^{13}C in $[TPPFe(^tBuNC)_2]^+$. The spectra were obtained as differences between those of the samples enriched with ^{13}C and the samples with a natural abundance of isotopes (∼1% of ^{13}C). Traces 1−5 are detected at $B_o = 3035$ ($g_{LF} = g_\perp = g_X = g_Y$), 3325, 3375, 3425, and 3495 G ($g_{HF} = g_{||} = g_Z$), respectively. The angles θ_{BZ} between $\mathbf{B_0}$ and $\mathbf{Z}$ corresponding to these B_o are shown at the left side of the figure. Experimental conditions: temperature, about 8 K; mw frequency, 9.445 GHz; mw pulse durations, 100 ns (180°), 50 ns (180°), and 100 ns (180°); time interval T between the first and second mw pulses, 60 μs; $\tau = 700$ ns; radio frequency pulse duration, $T_{RF} = 30$ μs. Dashed traces are simulated with $\rho_C = 0.079$, $\rho_{Fe} = 1 - 4\rho_C = 0.68$, $\theta_{pZ} = 21°$.

configuration of $[TPPFe(OCH_3)(OO\mathit{t}Bu)]^-$ is d_π and that the unusually small value of $\sum g^2$ observed for this complex probably arises from orbital quenching in this relatively weak-field anionic ligand system.

To understand the origin of the difference between the ENDOR spectra originating from Fe^{III}-porphyrinates with d_π and d_{xy} electron configurations, we must consider in some detail

the relation between the hyperfine interaction (hfi) parameters of *meso*-^{13}C and the spin density distributions in the porphyrin π-systems.

In the case of the d_{xy} electronic configuration, the main contributions to the *meso*-^{13}C hfi come from two sources. First, there is a dipole interaction between the electronic spin density ρ_{Fe} localized in the d_{xy} orbital and the magnetic moment of the *meso*-^{13}C nucleus. This interaction can be reasonably accounted for by using the point dipole approximation and is characterized by the anisotropic hfi coupling constant

$$T_{Fe} \approx -\rho_{Fe} g g_n \beta \beta_n / h (R_{FeC})^3 \quad (1)$$

which corresponds to the perpendicular component of the axially symmetric anisotropic hfi tensor. The axis of this tensor is directed along the radius-vector $\mathbf{R_{FeC}}$ connecting the central Fe^{3+} ion with the *meso*-carbon. The parameters entering eq 1 are as follows: g and g_n are, respectively, the electronic and nuclear g-factors; β and β_n are the Bohr magneton and the nuclear magneton, h is Planck's constant, and $R_{FeC} \approx 3.4$ Å. The value of T_{Fe} corresponding to $\rho_{Fe} = 1$ is about -0.5 MHz (at $g = 2$).

The other contribution to the hfi is from the π-spin density ρ_C localized on the *meso*-carbon itself. The anisotropic hfi is characterized by the axially symmetric tensor with perpendicular component $T_C \approx -50\rho_C$ MHz (at $g = 2$).[32,33] The axis of this tensor is directed along the carbon p-orbital, close to the heme normal **Z**, and is perpendicular (approximately, if the macrocycle is ruffled) to the axis of the hfi tensor determined by ρ_{Fe}. The isotropic hfi constant a_C resulting from ρ_C is about $100\rho_C$ MHz.[32,33]

The contributions of spin densities on other atoms in the porphyrin ring and, possibly, in the ligands, may be neglected because these spin densities are close to zero, as is also the case for the pyrrole carbons. In addition, other atoms are at fairly large distances from a given *meso*-carbon, and the spin densities on them are limited ($\rho < 0.1$[34]). Somewhat stretching the model, the spin densities on pyrrole nitrogens that are located close to the central Fe can be included in the effective value of ρ_{Fe}, which will only lead to a slight nonaxiality of the corresponding anisotropic hfi tensor, which has been neglected, and leads to a slightly overestimated value of ρ_{Fe}.

With the model formulated above, the total hfi constant $A_{||}$ corresponding to $\mathbf{B_o}//\mathbf{Z}$ can be written as

$$A_{||} = a_C + T_{Fe} - 2T_C \approx 100\rho_C - 0.25 g_Z \rho_{Fe} + 50 g_Z \rho_C \quad (2)$$

where all numerical factors are in megahertz, and the proportionality of the anisotropic hfi to the electronic g-factor is factored out. If $\mathbf{B_o} \perp \mathbf{Z}$, the hfi constant $A_\perp$ varies from

$$A_\perp = a_C + T_{Fe} + T_C \approx 100\rho_C - 0.25 g_\perp \rho_{Fe} - 25 g_\perp \rho_C \quad (3)$$

when $\mathbf{B_o} \perp \mathbf{R_{FeC}}$, to

$$A_\perp = a_C - 2T_{Fe} + T_C \approx 100\rho_C + 0.5 g_\perp \rho_{Fe} - 25 g_\perp \rho_C \quad (4)$$

when $\mathbf{B_o}//\mathbf{R_{FeC}}$. In eqs 3 and 4, $g_\perp$ is $g_{LF} = g_X = g_Y$.

To a first-order approximation in hfi, the two ^{13}C ENDOR lines are located at frequencies of $|\nu_C \pm A/2|$, where ν_C is the ^{13}C Zeeman frequency. Two situations are possible. In the weak coupling limit, when $\nu_C > A/2$, the doublet of ENDOR lines will be centered at ν_C and split by A. In the strong coupling limit, when $\nu_C < A/2$, the doublet will be centered at $A/2$ and split by $2\nu_C$. The doublet of ^{13}C lines seen in spectrum 5 of Figure 5 (near g_Z, $B_o = 3495$ G, $\nu_C \approx 3.74$ MHz) is centered at the frequency $\nu_{cnt} \approx 7.5$ MHz $> \nu_C$. It then clearly corresponds to the strong coupling case, and we can immediately estimate $A_{||} \approx 2\nu_{cnt} \approx 15$ MHz. Because the anisotropic hfi contribution from ρ_{Fe} is very small compared with $A_{||}$ (at $g = g_Z \approx 1.93$, $T_{Fe} \approx 0.48$ MHz, even at $\rho_{Fe} = 1$), it can be neglected in eq 2, and $\rho_C \approx 0.076$ can be readily estimated. If we include in the effective ρ_{Fe} all spin densities but those located on the *meso*-carbons (and for the d_{xy} system that virtually means only the spin densities on the pyrrole nitrogens), we may estimate $\rho_{Fe} \approx 1 - 4\rho_C \approx 0.7$.

Substituting $\rho_C \approx 0.076$ into eq 3 or 4 where, again, T_{Fe} is neglected, we can easily find $A_\perp \approx 3.4$ MHz. Using this value, the position of the high-frequency ^{13}C line, $\nu_C + A_\perp/2$, in the ENDOR spectrum at $g_\perp \approx 2.23$ can be estimated. The estimated frequency is about 4.95 MHz, very close to the maximum of the high-frequency line observed in the experimental spectrum 1 in Figure 5. Thus, it is seen that the ENDOR spectra recorded at both canonical orientations are successfully explained with this model for the hfi, which shows that it is reasonably accurate.

The ENDOR spectra recorded at B_o values other than those corresponding to the turning points of the EPR spectrum show ^{13}C transition frequencies intermediate between those observed at the turning points (see traces 2−4 in Figure 5). In addition, the high-frequency line in these spectra exhibits a splitting (we do not intend to discuss the low-frequency line, since it has a much lower intensity in the experimental spectra, and its shape is considerably affected by noise). This feature is interpreted as indicative of the p-orbitals of the *meso*-carbons (and their associated anisotropic hfi tensor axes) being not exactly parallel to **Z**. An alternative explanation with significantly inequivalent carbons fails because spectrum 5, recorded at g_Z, does not show resolved splittings, which indicates that the spin densities on all four *meso*-carbons are nearly identical.

To estimate the angle θ_{pZ} between **Z** and the axis of the *meso*-carbon p-orbital (assuming for simplicity θ_{pZ} to be the same for all four *meso*-carbons), numerical simulations of the ENDOR spectra have been performed with a variation of θ_{pZ}, ρ_C, and $\rho_{Fe} = 1 - 4\rho_C$. A reasonable fit was obtained for $\rho_C \approx 0.079$, $\rho_{Fe} \approx 0.68$, and $\theta_{pZ} \approx 21°$ (dashed traces in Figure 5). The spin density $\rho_C \approx 0.079$ found in this work for [*meso*-^{13}C-TPPFe(^{t}BuNC)$_2$]$^+$ is close to $\rho_C \approx 0.06$ found earlier for another d_{xy} system, [OEPFe(PhNC)$_2$]$^+$, using the ENDOR lines of the *meso*-protons.[35]

Now the *meso*-^{13}C ENDOR spectra of the d_π systems shown in Figure 4 will be considered briefly. The spectra recorded at g_Z show better (trace 1) or worse (trace 3) resolved sets of doublets (asymmetric in amplitude, probably, because of the implicit TRIPLE effect[36,37]) centered at the ^{13}C Zeeman

(32) Carrington, A.; McLachlan, A. D. *Introduction to Magnetic Resonance with Applications to Chemistry and Chemical Physics*; Harper and Row: New York, 1967.
(33) Landolt-Börnstein. In *Numerical Data and Functional Relationships in Science and Technology, New Series*; Madelung, O., Fisher, H., Eds.; Springer-Verlag: Berlin, 1987; Chapters 3,4, Vol. II/17b,c.
(34) Ghosh, A.; Gonzalez, E.; Vangberg, T. *J. Phys. Chem. B* **1999**, *103*, 1363−1367.
(35) Astashkin, A. V.; Raitsimring, A. M.; Kennedy, A. R.; Shokhireva, T. Kh.; Walker, F. A. *J. Phys. Chem. A* **2002**, *106*, 74−82.
(36) Doan, P. E.; Nelson, M. J.; Jin, H.; Hoffman, B. M. *J. Am. Chem. Soc.* **1996**, *118*, 7014−7015.

frequency and split by the hfi constants A_Z. Different doublet splittings indicate some inequivalence of the spin density distributions "seen" by different *meso*-carbons.

The main contribution to the *meso*-^{13}C anisotropic hfi in these systems is made by $\rho_{Fe} \approx 0.8$.[38] For example, for [*meso*-^{13}C-TPPFe(OCH$_3$)(OO^{t}Bu)]$^-$ ($g_Z \approx 2.3$), the corresponding anisotropic coupling constant T_{Fe} (see eq 1) is about 0.5 MHz. The spin densities on the *meso*-carbons are very small (≤ 0.003, according to our Hückel calculations), and may contribute no more than $T_C \approx -0.17$ MHz to the anisotropic hfi and $a_C \approx 0.3$ MHz to the isotropic hfi constant. Another important contribution to the hfi parameters of *meso*-^{13}C is made by the π-spin density ρ_α on the adjacent pyrrole α-carbons. The contribution from ρ_α to the isotropic hfi of *meso*-^{13}C may be estimated as $a_\alpha \approx -35\rho_\alpha$ MHz.[39] With ρ_α reaching 0.015 it may be as large as -0.6 MHz, and with two pyrrole α-carbons neighboring each *meso*-^{13}C, $a_\alpha \approx -1$ MHz is a reasonable estimate. The anisotropic hfi contribution of $\rho_\alpha \approx 0.015$ may be roughly estimated in the point dipole approximation to give the coupling constant $T_\alpha \approx -0.13$ MHz.

It can be seen that the main contributions to the total hfi constant A_Z of the *meso*-^{13}C are the isotropic contribution of spin densities ρ_α on adjacent pyrrole α-carbons ($a_\alpha \approx -1$ MHz) and the anisotropic contribution from ρ_{Fe} ($T_{Fe} \approx -0.5$ MHz at $g = g_Z \approx 2.3$). The sum of these contributions gives $A_Z \approx -1.5$ MHz, which correlates with the maximal splitting of about 1.7 MHz observed in spectrum 1 in Figure 4. In spectrum 3, which corresponds to that at $g_Z \approx 2.83$ of [*meso*-^{13}C-TPPFe(N-MeIm)$_2$]$^+$, the maximal splitting is very similar, about 1.6 MHz. In spectra 2 and 4 recorded at $g_{HF} = g_X$, the maximal splittings are, naturally, of similar magnitude, about 1.05 MHz in trace 2 ($g_{HF} \approx 1.95$) and about 0.9 MHz in trace 4 ($g_{HF} \approx 1.53$). The general structure of various *meso*-^{13}C hfi contributions is thus understood. However, the numerous possible contributions prohibit any detailed analysis of the ENDOR spectra in Figure 4 aimed at extracting the exact spin densities on the *meso*- and pyrrole α-carbons.

An important parameter that will be used below in the discussion of the ^{13}C NMR isotropic shifts is the ratio of the isotropic hfi constants a_{meso} of *meso*-^{13}C in the d_{xy} and d_π configurations. With $\rho_C \approx 0.08$ estimated above for the d_{xy} configuration, a_{meso} is about 8 MHz. For the d_π configuration, as discussed above, a_{meso} is mostly determined by the spin polarization contributions from the pyrrole α-carbons and is close to -1 MHz. The ratio of the hfi constants is thus in the range from -8 to -10.

To conclude the discussion of the *meso*-^{13}C ENDOR spectra, it can be mentioned here that they, indeed, show in a very straightforward way the gross features of spin density distribution over the porphyrin ring related to the particular electronic configuration of the iron-porphyrin complex, and may be used to make the corresponding assignments.

^{13}C NMR Spectroscopy Reveals that [TPPFe(OCH$_3$)(OO^{t}Bu)]$^-$ Has a d_{xy} Electron Configuration at 193 K and, by Extrapolation, at Room Temperature. The picture that emerges from ^{13}C NMR spectroscopic studies over the temperature range 178−218 K is very different from that discussed above for the ^{13}C pulsed ENDOR measurements carried out at 8 K. The ^{13}C NMR spectrum obtained from a solution of [*meso*-^{13}C-TPPFe(OCH$_3$)(OO^{t}Bu)]$^-$ at 193 K is shown in Figure 6A(a). The observed chemical shift for the *meso*-carbon is 422 ppm. The relevance of this chemical shift becomes evident if one considers that it has recently been shown that the *meso*-carbon chemical shift of ^{13}C-labeled ferrihemes is an excellent diagnostic tool for differentiating between the d_π and d_{xy} electron configuration.[40] Complexes with the d_π unpaired electron configuration have small chemical shifts (tens of ppm),[41] whereas those with the unpaired electron in the d_{xy} orbital typically exhibit large chemical shifts (hundreds of ppm).[40,42] For instance, the chemical shift observed for [*meso*-^{13}C-TPPFe(ImH)$_2$]$^-$ is 12 ppm at 193 K (see below), while that of [*meso*-^{13}C-TPPFe(^{t}BuNC)$_2$]$^+$ is estimated[43] to be somewhat greater than 1000 ppm at 193 K (see below). The chemical shift observed for [*meso*-^{13}C-TPPFe(OCH$_3$)(OO^{t}Bu)]$^-$ is somewhat less than the average of the two (516 ppm), suggesting a significant population of the d_{xy} electron configuration at 193 K, and a small energy difference between the d_π and d_{xy} electron configurations.[44]

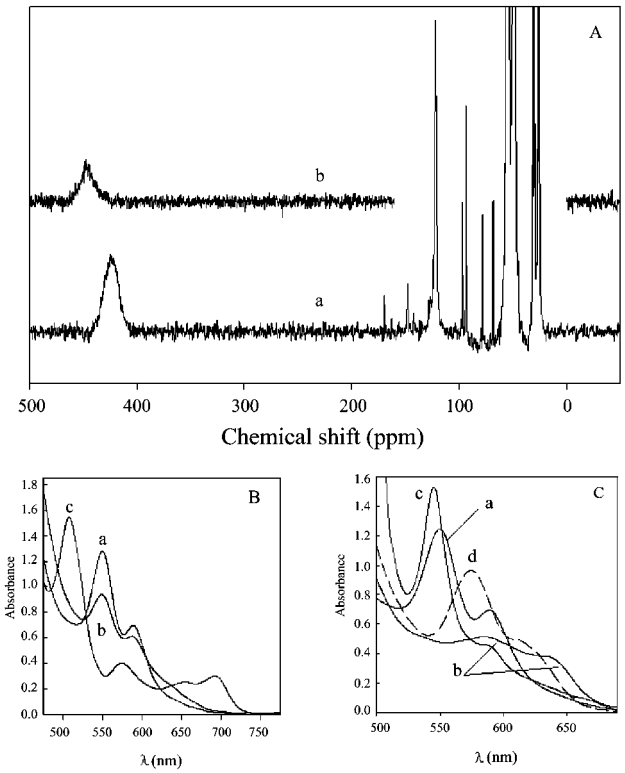

Figure 6. (A) (a) ^{13}C NMR spectrum of [*meso*-^{13}C-TPPFe(OCH$_3$)(OO^{t}Bu)]$^-$ obtained at 193 K, and (b) of high-spin TPPFe(OCH$_3$) in toluene-d_8 at 195 K. (B) Electronic absorption spectra of [TPPFe(OCH$_3$)(OO^{t}Bu)]$^-$ at (a) 195 K, (b) after 3 h at 231 K, (c) spectrum obtained from TPPFeCl at 195 K. (C) Electronic absorption spectra of (a) [TPPFe(OCH$_3$)(OO^{t}Bu)]$^-$, (b) [TPPFe(OCH$_3$)$_2$]$^-$, (c) [TPPFe(OO^{t}Bu)$_2$]$^-$, and (d) spectrum obtained from TPPFe(OCH$_3$) in benzene at room temperature.

(37) Astashkin, A. V.; Raitsimring, A. M.; Walker, F. A. *J. Am. Chem. Soc.* **2001**, *123*, 1905−1913.
(38) Scholes, C. P.; Falkowski, K. M.; Chen, S.; Bank, J. *J. Am. Chem. Soc.* **1986**, *108*, 1660−1671.
(39) Zhidomirov, G. I.; Schastnev, P. V.; Chuvylkin, N. D. *Quantum-Chemical Calculations of Magnetic-Resonance Parameters*; Nauka: Novosibirsk, 1978.
(40) Ikeue, T.; Ohgo, Y.; Takashi, S.; Nakamura, M.; Fujii, H.; Yokoyama, M. *J. Am. Chem. Soc.* **2000**, *122*, 4068−4076.
(41) Goff, H. M. *J. Am. Chem. Soc.* **1981**, *103*, 3714−3722.
(42) Ikewue, T.; Ohgo, Y.; Saitoh, T.; Yamaguchi, T.; Nakamura, M. *Inorg. Chem.* **2001**, *40*, 3423−3434.
(43) The signal broadens and disappears below 258 K, probably because of slowing of the ruffled porphyrinate inversion kinetics.
(44) Shokhirev, N. V.; Walker, F. A. *J. Phys. Chem.* **1995**, *99*, 17795−17804.

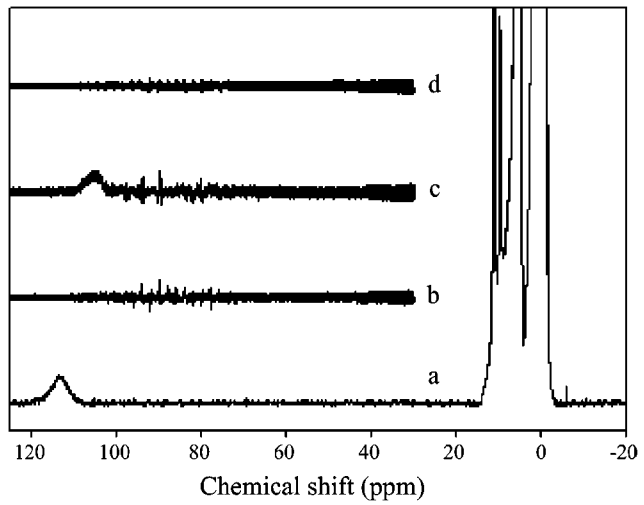

Figure 7. 400 MHz ^{1}H NMR spectra of (a) TPPFe(OMe) in toluene d_8 at −70 °C; (b) [*meso*-^{13}C-TPPFe(OCH$_3$)(OO^{t}Bu)]$^-$ at −80 °C; (c) [*meso*-^{13}C-TPPFe(OCH$_3$)$_2$]$^-$ at −70 °C; and (d) *meso*-^{13}C-TPPFe(OO^{t}Bu)$_2$]$^-$ at −80 °C. The latter three complexes were prepared with nondeuterated methanol and TMAOH, as described in the Experimental Section. Thus the corresponding spectra were acquired with fast repetition rates (50 ms acquisition time, 16 k data points, and 100 kHz spectral width) to minimize the intensity of the long-lived signals. Short acquisition times result in truncation of the intense methanol and TMOH signals, which upon Fourier transformation impart a slight beating pattern to the baseline. The presence of a pyrrole-H signal near 100 ppm in spectrum (c) indicates that the complex labeled "[TPPFe(OMe)$_2$]$^-$" is a mixture of high-spin TPPFe(OMe) and low-spin [TPPFe(OMe)$_2$]$^-$. In contrast, spectra (b) and (d) indicate the absence of detectable high-spin species in equilibrium with [TPPFe(OMe)(OO^{t}Bu)]$^-$ and [TPPFe(OO^{t}Bu)$_2$]$^-$.

Before the electronic configuration of [*meso*-^{13}C-TPPFe(OCH$_3$)(OO^{t}Bu)]$^-$ can be assigned with complete certainty at 193 K, it is important to consider alternative explanations of the large ^{13}C chemical shift observed for this complex. For example, it is necessary to exclude the possibility that at 193 K [TPPFe(OCH$_3$)(OO^{t}Bu)]$^-$ is in equilibrium with a high-spin species such as five-coordinate TPPFe(OCH$_3$) or TPPFe(OO^{t}Bu). Fe^{III} porphyrinates coordinated by a single anionic ligand are known to display *meso*-carbon chemical shifts in the range from 300 to 500 ppm at ambient temperatures.[45,46] The ^{13}C NMR spectrum at 195 K of *meso*-^{13}C-TPPFe(OCH$_3$), prepared in toluene-d_8, is presented in Figure 6A(b), and the ^{1}H NMR spectrum of this same high-spin mono-methoxy complex at the same temperature is shown in Figure 7a. The ^{1}H NMR spectrum displays a pyrrole-H resonance at 114 ppm. This pyrrole-H chemical shift is very similar to that reported for the hydroxy complex,[47] as well as the well-known chloride complex,[47] and is uniquely indicative of a high-spin Fe(III) complex. Hence, the mono-methoxy complex prepared in our laboratories is indeed high-spin. Therefore, the ^{13}C shift of the *meso*-^{13}C TPPFe(OCH$_3$) (Figure 6A(b)) is characteristic of those to be expected for high-spin complexes related to this study. Because of the similarity in chemical shift of the high-spin TPPFe(OCH$_3$) complex (Figure 6A(b)) to that for the [*meso*-^{13}C-TPPFe(OCH$_3$)(OO^{t}Bu)]$^-$ of Figure 6A(a), it must be established whether at 193 K the latter is indeed a low-spin complex. Pertinent evidence is provided by the fact that the electronic absorption spectrum of a cherry red solution of [TPPFe(OCH$_3$)(OO^{t}Bu)]$^-$ at 195 K (Figure 6B(a)), with well-resolved α and β bands, is clearly characteristic of a low-spin Fe^{III} porphyrinate.[48] This electronic spectrum is clearly distinct from the electronic spectra of high-spin Fe^{III} porphyrinates, such as those corresponding to TPPFeCl (Figure 6B(c)) and TMPFe(OO^{t}Bu) (Figure 4 in ref 48). The electronic absorption spectrum of the high-spin TPPFe(OCH$_3$) (reported previously[49]) (Figure 6C(d)) is rather different from those corresponding to TPPFeCl and TMPFeOO^{t}Bu, and is similar in structure to those characteristic of low-spin porphyrinates, in that it has two visible bands. However, the wavelength maxima of these two bands are markedly different from those displayed by the spectrum of the low-spin complex, [TPPFe(OCH$_3$)(OO^{t}Bu)]. Moreover, the electronic absorption spectrum of the latter (Figure 6B(a,b)) is almost identical to that reported by Tajima and co-workers in a frozen glass at 77 K,[18,19] while, at the same time, the EPR spectrum detected at 77 K is characteristic of a low-spin iron(III) porphyrinate complex. These observations strongly suggest that [*meso*-^{13}C-TPPFe(OCH$_3$)(OO^{t}Bu)]$^-$ is a low-spin complex at 195 K, as well as at 77 K.[17,18] Additional evidence corroborating the low-spin nature of [*meso*-^{13}C-TPPFe(OCH$_3$)(OO^{t}Bu)]$^-$ stems from its ^{1}H NMR spectrum at 193 K (Figure 7b), which unequivocally shows the absence of pyrrole-H resonances that are diagnostic of high-spin porphyrinates. The low-spin nature of the complex having been established, one can conclude that the chemical shift of the *meso*-carbon, 422 ppm at 193 K, clearly indicates that the [TPPFe(OCH$_3$)(OO^{t}Bu)]$^-$ complex at this temperature has at least partial d_{xy} electron configuration. The question of the degree of population of the d_{xy} electronic state is dealt with in the next section.

Variable Temperature ^{13}C NMR Spectroscopy of [*meso*-TPPFe(OCH$_3$)(OO^{t}Bu)]$^-$ Indicates a Thermodynamic Equilibrium between Electron Configurations. To explore the temperature dependence of the *meso*-carbon resonance in [*meso*-^{13}C-TPPFe(OCH$_3$)(OO^{t}Bu)]$^-$, it was necessary to first establish the temperature range over which [TPPFe(OCH$_3$)(OO^{t}Bu)]$^-$ is stable. It was also necessary to determine whether changes in temperature result in equilibria of [TPPFe(OCH$_3$)(OO^{t}Bu)]$^-$ with other species. Examples of such chemical species are the high-spin complexes TPPFe(OCH$_3$) and TPPFe(OO^{t}Bu) mentioned above, and the low-spin bis-ligand complexes [TPPFe(OCH$_3$)$_2$]$^-$ and [TPPFe(OO^{t}Bu)$_2$]$^-$. Electronic absorption and ^{1}H NMR spectroscopies were again useful in answering these questions. The electronic absorption spectrum of [TPPFe(OCH$_3$)(OO^{t}Bu)]$^-$ at 212 K (CHCl$_3$-dry ice bath) is very similar to that obtained at 195 K (Figure 6B(a)), thus providing strong evidence that the system does not undergo an equilibrium involving a change in spin state and that it does not decompose at this temperature. The solution containing [TPPFe(OCH$_3$)(OO^{t}Bu)]$^-$ was warmed to 231 K (CH$_3$CN-dry ice) for 3 h. The resultant electronic absorption spectrum (Figure 6B(b)) is identical in features to those obtained at 212 and 195 K, but is less intense. We interpret these results as indicating that at temperatures above 212 K it is likely that the alkyl peroxide reacts with the porphyrin to produce oxidation products that

(45) Mispelter, J.; Momenteau, M.; Lhoste, J. M. *Chem. Commun.* **1979**, 808−810.
(46) Goff, H. M.; Shimomura, E. T.; Phillippi, M. A. *Inorg. Chem.* **1983**, *22*, 66−71.
(47) Cheng, R.-J.; Latos-Grazynski, L.; Balch, A. L. *Inorg. Chem.* **1982**, *21*, 2412−2418.
(48) Arasasingham, R. D.; Cornman, C. R.; Balch, A. L. *J. Am. Chem. Soc.* **1989**, *111*, 7800−7805.
(49) Kobayashi, H.; Higuchi, T.; Kaizu Y.; Osada, H.; Aoki, M. *Bull. Chem. Soc. Jpn.* **1975**, *48*, 3137−3141.

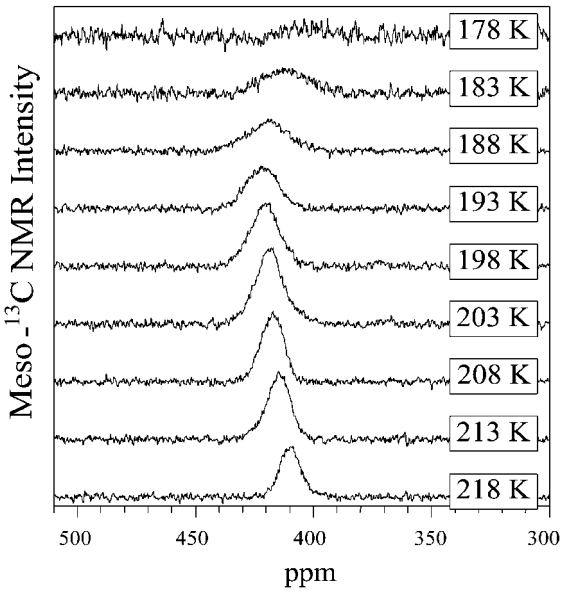

Figure 8. ^{13}C NMR spectra of [*meso*-^{13}C-TPPFe(OCH$_3$)(OO^{t}Bu)]$^-$, obtained at different temperatures (listed at the right side of the figure), over 16 k data points, with a spectral width of 8.6 kHz, 90 ms acquisition time, 40 ms relaxation delay, and 40 000 scans.

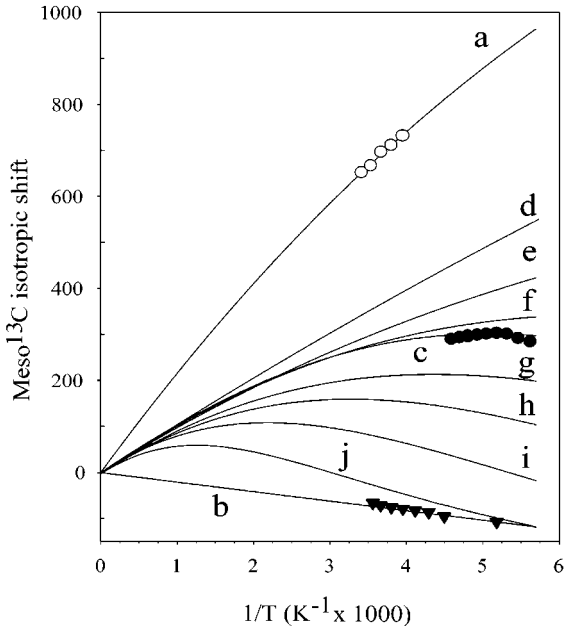

Figure 9. Temperature dependence of the *meso*-^{13}C isotropic shift (δ_{iso} = chemical shift − δ_{dia} (120 ppm[41])) for several complexes (as indicated in the figure), with fits for (a) a "pure" d_{xy} electron configuration; (b) a "pure" d_π electron configuration; (c) a chemical equilibrium between the two data points (●) for the ($^-$OCH$_3$)($^-$OO^{t}Bu) complex; and a thermally accessible excited state, either (d) 20 cm^{-1}, (e) ∼50 cm^{-1}, (f) 100 cm^{-1}, (g) 150 cm^{-1}, (h) 200 cm^{-1}, (i) 300 cm^{-1}, or (j) 520 cm^{-1} above the ground state. In plots a−j, the diamagnetic chemical shift of the *meso*-C was taken as 120 ppm, as obtained experimentally by Goff for [TPPCo(N-MeIm)$_2$]$^+$.[39]

are much less intensely colored, hence decreasing the absorption intensity. Nevertheless, the spectrum in Figure 6B(b) clearly indicates the absence of a high-spin species at 212 K. On the basis of these observations, it was decided to study [*meso*-^{13}C-TPPFe(OCH$_3$)(OO^{t}Bu)]$^-$ between 218 and 178 K. The upper limit is imposed by the reactivity of the alkyl peroxide ligand and the lower limit by the freezing point of the solvent.

The ^{1}H NMR spectra of [TPPFe(OCH$_3$)(OO^{t}Bu)]$^-$ obtained every 10 K between 178 and 218 K are similar to the spectrum shown in Figure 7b in that peaks diagnostic of pyrrole-H resonances, which typically resonate between 70 and 120 ppm, depending on temperature, are completely absent. In addition, electronic absorption spectra obtained at different temperatures (see Figure 6B) also allowed us to conclude that neither the 5-coordinate high-spin TPPFe(OCH$_3$) or TPPFe(OO^{t}Bu), nor the six-coordinate low-spin [TPPFe(OO^{t}Bu)$_2$]$^-$ or [TPPFe(OCH$_3$)$_2$]$^-$, complexes exist in detectable concentrations under the conditions used to study [*meso*-^{13}C-TPPFe(OCH$_3$)(OO^{t}Bu)]$^-$. Evidence supporting the absence of low-spin complexes other than [TPPFe(OCH$_3$)(OO^{t}Bu)]$^-$ is shown in Figure 6C. The electronic absorption spectrum of [TPPFe(OCH$_3$)(OO^{t}Bu)]$^-$ (Figure 6C(a)) is clearly distinct from the spectra originating from both [TPPFe(OCH$_3$)$_2$]$^-$ and [TPPFe(OO^{t}Bu)$_2$]$^-$, Figure 6C(b) and 6C(c), respectively. Furthermore, the spectrum characteristic of [TPPFe(OO^{t}Bu)$_2$]$^-$ can only be observed upon addition of a 600-fold molar excess of ^{t}BuOOH with respect to TPPFeCl (1 TPPFeCl (0.2 mM):200 OH$^-$:600 ^{t}BuOOH). By comparison, [TPPFe(OCH$_3$)(OO^{t}Bu)]$^-$ is prepared by the addition of a 100-fold molar excess of ^{t}BuOOH with respect to TPPFeCl (1 TPPFeCl (0.2 mM):200 OH$^-$:100 ^{t}BuOOH).

When [*meso*-^{13}C-TPPFe(OCH$_3$)(OO^{t}Bu)]$^-$ is cooled from 218 to 193 K, the *meso*-carbon shift increases, as is expected for a low-spin ferriheme center possessing the d_{xy} electron configuration. However, below 193 K the direction reverses, and the *meso*-carbon chemical shift decreases rapidly and becomes increasingly broader (Figure 8). The temperature dependence of the *meso*-carbon chemical shift, shown by ● in Figure 9, was fit to different models. To consider the possibility of a thermally accessible excited state, the following equation for the contact shift was used:[16,44]

$$\delta_n^{\,con} = (F/T)\{W_1 C_{n1}{}^2 + W_2 C_{n2}{}^2 e^{-\Delta E/kT}\}/\{W_1 + W_2 e^{-\Delta E/kT}\} \quad (5)$$

where δ_n^{con} is the contact shift of the *meso*-carbon, F is the Curie factor that relates the contact shift to the orbital coefficients, T is the absolute temperature, W_1 and W_2 are the weighting factors for the ground and excited state orbitals, respectively (equal in this case because both have spin $S = {}^1/_2$), C_{n1} and C_{n2} are the orbital coefficients for position n in the ground (1) and excited (2) states, respectively, ΔE is the energy separation between ground and excited states, and k is the Boltzmann constant. For the present case, since the direction of shift is opposite for the d_{xy} and d_π electronic states of low-spin Fe(III) (Figure 9a and b, respectively), the carbon orbital coefficients are obviously very different−of opposite sign, in fact. Thus, the coefficients $C_{n1}{}^2$ and $C_{n2}{}^2$ in eq 5 must include the product of the spin densities at the meso position in each state and the sensitivity of the spin density to the various orbital contributions. On the basis of the ratio of the isotropic hfi constants of *meso*-^{13}C in d_{xy} and d_π configurations estimated above from ^{13}C ENDOR spectra and from spin polarization considerations,[41,50] we can take $C_{n2}{}^2/C_{n1}{}^2$ to be ∼−10, with $C_{n1}{}^2$ being negative.

Fits of the temperature dependence of the ^{13}C isotropic shifts to eq 5, first of all for the two "pure" complexes, [*meso*-^{13}C-

(50) Karplus, M.; Fraenkel, G. K. *J. Chem. Phys.* **1961**, *35*, 1312−1323.

TPPFe(^{t}BuNC)$_2$]$^+$ (d_{xy}) (○ in Figure 9) and [TPPFe(ImH)$_2$]$^+$ (d_π) (▼ in Figure 9), show that each has a thermally accessible excited state of the opposite electron configuration, with the energy between ground and excited states, $\Delta E \approx 97$ and 417 cm^{-1}, respectively. Thus, both of the ^{13}C isotropic shift lines of the "pure" complexes in Figure 9 are slightly curved, with that for the d_{xy} electron configuration (a) being more curved than that for the d_π electron configuration (b). The average of the isotropic shifts of the two "pure" electron configurations is shown in Figure 9 by plot (e). Plot (e) corresponds not only to the simple average of the chemical shifts for the two "pure" electron configurations, but also to that calculated from eq 5 for $\Delta E \approx 50$ cm^{-1}. Not only the strict average (e) of the two "pure" electron configurations, but also the calculated temperature dependence based upon a variety of ΔE values, including 20 cm^{-1} (d), 100 cm^{-1} (f), 150 cm^{-1} (g), 200 cm^{-1} (h), 300 cm^{-1} (i), and a very large $\Delta E = 520$ cm^{-1} (j) as possible values for the temperature dependence of [*meso*-^{13}C-TPPFe(OCH$_3$)-(OO^{t}Bu)]$^-$ are shown. All lines d−j were calculated from eq 5 using the ratio $C_{n2}^2/C_{n1}^2 = -10$, as discussed above.

The markedly different behavior of the experimental *meso*-carbon chemical shift (● in Figure 9) and those expected for a thermally accessible excited state clearly demonstrates that the temperature dependence of [*meso*-^{13}C-TPPFe(OCH$_3$)(OO^{t}Bu)]$^-$ is not that expected for a system having a thermally accessible excited state. In particular, the isotropic shifts reach a maximum at a particular value of inverse temperature, and then decrease. The maximum isotropic shift is reached at a relatively low temperature, 193 K, unlike that for any possible value of ΔE, for which only those cases having $\Delta E = 150$ cm^{-1} or greater reach a very gentle maximum isotropic shift before decreasing, and the temperatures at which these maxima are reached are all greater than 193 K. However, the approximate similarity of the experimental data points for this complex to the calculated behavior if there were a thermally accessible excited state with $\Delta E = 100$ cm^{-1} or so suggests that it is highly likely that these two electron configurations have a very small difference in energy. In fact, it was not possible to fit the experimental temperature dependence of [*meso*-^{13}C-TPPFe(OCH$_3$)(OO^{t}Bu)]$^-$ without also considering the existence of a thermodynamic equilibrium that shifts in favor of the d_{xy} electron configuration as the temperature is raised. As a first estimation of the equilibrium constants for such a process, the *meso*-^{13}C chemical shifts of this complex were compared to those of complexes with "pure" electron configurations, [TPPFe(ImH)$_2$]$^+$ for the d_π, and [TPPFe(^{t}BuNC)$_2$]$^+$ for the d_{xy} electron configuration. It can be readily shown that for the ring conformation interconversion,

$$\text{planar}\,(d_\pi) \overset{K_{eq}}{\rightleftharpoons} \text{ruffled}\,(d_{xy}) \tag{6}$$

$$K_{eq} = |\delta(\text{pure}\,d_\pi) - \delta(\text{peroxo})|/|\delta(\text{pure}\,d_{xy}) - \delta(\text{peroxo})| \tag{7}$$

Hence, K_{eq} can be easily estimated, and then a van't Hoff plot (log K_{eq} vs $1/T$) can be constructed to estimate the ΔH and ΔS for this interconversion. Values of $\Delta H \approx +2.53 \pm 0.5$ kJ/mol and $\Delta S \approx +12 \pm 4$ J/mol K are obtained from the best slope and intercept of this plot. These values can then be used in an expression similar to that of eq 5, but appropriate for a thermodynamic equilibrium, with enthalpy ΔH and entropy ΔS, to calculate the contact shift for the *meso*-carbon of the alkyl peroxide complex as a function of temperature:

$$\delta_n^{\,con} = (F/T)\{C_{n1}{}^2 + C_{n2}{}^2 e^{-(\Delta H - T\Delta S)/RT}\}/\{1 + e^{-(\Delta H - T\Delta S)/R}\} \tag{8}$$

Using the same values of $C_{n1}{}^2$ and $C_{n2}{}^2$, and the estimated values of $\Delta H \approx +2.53$ kJ/mol and $\Delta S \approx +12$ J/mol K, plot (c) in Figure 9 is obtained. This plot more closely follows the chemical shift dependence of the experimental data points than do the plots obtained from the assumption of a thermally accessible excited state using any value of ΔE between ground and excited state (eq 5), in that the curve reaches a maximum at the point that the experimental data reach a maximum, and then decreases, albeit at a less rapid rate than do the experimental data (see below).

Although both metal- and ligand-centered dipolar shifts are also expected to contribute to the isotropic shifts[41] of the low-spin Fe(III) complexes of this study, their contributions are much smaller than those of the contact shifts, and they likely mirror those of the contact shifts in these complexes in solution where the ligands within each complex ion, as well as the complex ions themselves, are rotating rapidly. Thus, it is felt that within the accuracy of the approximate calculations for lines c−j of Figure 9, the dipolar shift contributions will not change the overall picture. Therefore, the results summarized in Figure 9 are consistent with the fact that the temperature dependence of the chemical shift obtained from [*meso*-^{13}C-TPPFe(OCH$_3$)-(OO^{t}Bu)]$^-$ results from a chemical equilibrium between planar (d_π) and ruffled (d_{xy}) conformations, for which the energy of the two electronic configurations is very nearly the same, but there is a thermodynamic equilibrium between the planar and ruffled ring conformations. The small values of both ΔH and ΔS are consistent with such an equilibrium between species that differ in ring conformation.

Both the extreme broadening and the stronger than predicted decrease in chemical shift at the lowest temperatures accessible in the solvent (188−178 K, last three points of line (c) in Figure 9) suggest an approach to the intermediate exchange regime. If this is the case, then at considerably lower temperatures, if the solvent did not freeze, the planar and ruffled conformers would be in slow exchange with respect to the NMR time scale, and two *meso*-carbon signals, one from each complex, would be observed. One signal would approach the chemical shift of the planar d_π complex and would become more intense, while the other signal would approach the chemical shift of the ruffled d_{xy} complex and become less intense, until it disappeared. Hence, the temperature dependence of the *meso*-carbon chemical shift (● in Figure 9) does not contradict the fact that at 8 K the pulsed ENDOR results (Figure 4) clearly indicate a d_π electron configuration. Thus, if the evidence gathered by electronic and magnetic spectroscopy is taken together, it can be concluded that at very low temperatures the electron configuration of [TPPFe(OCH$_3$)(OO^{t}Bu)]$^-$ is indeed d_π, but that the d_{xy} configuration becomes highly favored at ambient temperatures via a chemical equilibrium. Over the range of temperatures of the NMR measurements, both electronic states are present and rapidly interconverting, and at physiologically relevant temperatures, the d_{xy} electron configuration is expected to be strongly favored ($\Delta G_{310} = -1.19$ kJ/mol, $K_{eq} \approx 6.9$).

Magnetic Resonance Spectroscopy of $[TPPFe(OCH_3)_2]^-$ and $[TPPFe(OO^tBu)_2]^-$. The EPR spectra of $[TPPFe(OCH_3)_2]^-$ and $[TPPFe(OO^tBu)_2]^-$ also display compressed *g* anisotropy ($\sum g^2 \approx 14$), as shown in Figure 3. This observation raised the possibility that the bis-methoxide and bis-alkyl peroxide complexes of TPPFe(III) might have d_{xy} electron configurations. Hence, both complexes were also studied by pulsed ENDOR and ^{13}C NMR spectroscopy. The pulsed ENDOR results, summarized in Supporting Information Figure S1, show that the hyperfine splittings in the spectra obtained from [*meso*-^{13}C-$TPPFe(OCH_3)_2]^-$ and [*meso*-^{13}C-$TPPFe(OO^tBu)_2]^-$ are very similar to those of $[TPPFe(OCH_3)(OO^tBu)]^-$ and $[TPPFe(N\text{-}MeIm)_2]^+$ (d_π) in Figure 4, and also do not exceed 1.7 MHz. The magnitude of these hyperfine splittings is thus typical of complexes having their unpaired electron residing in a d_π orbital, as discussed above for $[TPPFe(OCH_3)(OO^tBu)]^-$. It is therefore evident that both $[TPPFe(OCH_3)_2]^-$ and $[TPPFe(OO^tBu)_2]^-$ have $(d_{xy})^2(d_{xz},d_{yz})^3$ electron configurations at 8 K.

The *meso*-carbon chemical shifts obtained for [*meso*-^{13}C-$TPPFe(OCH_3)_2]^-$ and [*meso*-^{13}C-$TPPFe(OO^tBu)_2]^-$ at 193 K are 361 and 444 ppm, respectively. Before the magnitude of these chemical shifts can be taken as an indication that the corresponding compounds are low-spin ferriheme complexes possessing an electron configuration in which the d_{xy} and d_π states are essentially isoenergetic, it is necessary to establish that these compounds are not in equilibrium with high-spin species such as $TPPFe(OCH_3)$ and $TPPFe(OO^tBu)$. Once again, electronic absorption spectroscopy and ^1H NMR spectroscopy were utilized to study these compounds. The electronic absorption spectrum of the olive green solution of $[TPPFe(OCH_3)_2]^-$ (Figure 6C(b)) was found to be temperature independent between 273 and 183 K; temperatures above 273 K were not investigated. It is noteworthy, however, that the electronic absorption spectra of $[TPPFe(OCH_3)_2]^-$ in this temperature range are somewhat different from those obtained by Tajima et al.[18] at 77 K. Interestingly, ^1H NMR spectra acquired from solutions of "$[TPPFe(OCH_3)_2]^-$" in this range of temperatures display a pyrrole-H peak near 100 ppm that is diagnostic of high-spin ferrihemes. For example, at 203 K the pyrrole-H resonance originating from "$[TPPFe(OMe)_2]^-$" is located at 100 ppm (see Figure 7c). By comparison, the pyrrole-H peak obtained from a sample of authentic high-spin TPPFe(OMe) in toluene (203 K) is found at 114 ppm (Figure 7a). Similar observations at other temperatures suggest that at 203 K the compound labeled "$[TPPFe(OMe)_2]^-$" is indeed a mixture of high-spin TPPFe(OMe) and low-spin $[TPPFe(OMe)_2]^-$. The presence of a detectable equilibrium between high-spin monomethoxy and low-spin bis-methoxy complexes in solution precludes any further analysis of this complex.

In contrast, the electronic absorption spectrum of a cherry red solution of $[TPPFe(OO^tBu)_2]^-$ (Figure 6C(c)) is different from the spectra displayed by the high-spin TPPFeCl, TPPFe(OMe), and $TMPFe(OO^tBu)$[48] complexes. The electronic absorption spectrum of $[TPPFe(OO^tBu)_2]^-$ loses intensity relatively rapidly above 195 K; thus ^1H and ^{13}C NMR experiments aimed at elucidating the spin state and electronic structure of [*meso*-^{13}C-$TPPFe(OO^tBu)_2]^-$ were acquired only between 203 and 178 K. In this range of temperatures, the ^1H NMR spectra of this complex, see Figure 7d for an example, are devoid of peaks near 100 ppm, thus indicating the absence of detectable quantities of high-spin species in solution. These observations indicate that [*meso*-^{13}C-$TPPFe(OO^tBu)_2]^-$ is a low-spin complex, and, hence, the magnitude of its *meso*-carbon chemical shifts is indicative of a d_{xy} electronic structure. The temperature dependence of the *meso*-carbon chemical shifts, together with those obtained from the variable temperature experiments performed with [*meso*-^{13}C-$TPPFe(OCH_3)(OO^tBu)]^-$, are shown in Supporting Information Figure S2. The temperature dependence of the *meso*-carbon in [*meso*-^{13}C-$TPPFe(OO^tBu)_2]^-$ indicates that in the temperature range accessible experimentally, the *meso*-carbon chemical shift moves to higher frequency as the temperature is decreased. This is what is expected for a low-spin ferriheme complex with a d_{xy} electron configuration. However, since pulsed ENDOR spectroscopy indicates that the electron configuration of this complex at 8 K is d_π, it is anticipated that the direction of the *meso*-carbon chemical shift will reverse at a lower (inaccessible) temperature. Hence, the plots in Figure S2 are qualitatively indicative of the relative position of the equilibrium between the d_{xy} (ruffled) and d_π (planar) conformations. These plots suggest that as the number of alkyl peroxide axial ligands is increased from one to two, the relative concentration of the d_{xy} conformer is larger at the lowest temperatures accessible experimentally. It is therefore likely that other ferriheme complexes with EPR spectra similar to those shown in Figure 3, including the imidazolate complex $[TPPFe(Im)(OO^tBu)]^-$[19] and the neutral imidazole complex $[TPPFe(N\text{-}MeIm)(OO^tBu)]$,[51] will also display variable temperature *meso*-carbon chemical shifts similar to those observed for the alkoxide-alkyl peroxide and bis-alkyl peroxide complexes of $TPPFe^{III}$ reported here, yet different in detail because of different ligand field strength of the unique axial ligand. This possibility is currently under investigation in our laboratories.

Relevance to Enzyme Systems and Concluding Remarks

In addition to the complexes included as part of this study, the EPR spectrum of the Fe^{III}-OOH complex of myoglobin ($\sum g^2 = 14.09$)[11,24,52] and that of the Fe^{III}-OOH complex of cytochrome $P450_{cam}$ ($\sum g^2 = 13.75$)[23,24] display compressed *g* anisotropy and very similar *g*-values to those reported for the corresponding alkyl peroxide complexes. These molecules have in common a hydroperoxide or alkyl peroxide axial ligand. Thus it seems obvious that the peroxide ligand induces the reduced anisotropy observed in the EPR spectra. Compressed *g* anisotropy *could* be correlated to a $(d_{xz},d_{yz})^4(d_{xy})^1$ electronic configuration in those cases, or, as in the model heme systems studied herein, the electron configuration at the very low temperatures utilized to carry out EPR spectroscopic studies is $(d_{xy})^2(d_{xz},d_{yz})^3$, with the possibility that some or all of these ferriheme centers coordinated by a peroxide ligand have a $(d_{xz},d_{yz})^4(d_{xy})^1$ electron configuration at ambient temperatures. This has important implications for the mechanism of action of the enzymes heme oxygenase, cytochromes P450, and the peroxidases, since the formation of an obligatory Fe^{III}-OOH intermediate, possessing large electron and spin density at the meso positions, can be expected to prime a protein or enzyme to oxygenate its heme.

(51) Rivera, M.; Caignan, G.; Astashkin, A. V.; Raitsimring, A. M.; Shokhireva, T. Kh.; Walker, F. A., unpublished work.
(52) Kappl, R.; Höhn Berlage, M.; Hütterman, J.; Bartlett, N.; Symons, M. C. R. *Biochim. Biophys. Acta* **1985**, *827*, 327−343.

Therefore, the ability of a protein to form the important "Fe(V)" and ferryl (Fe^{IV}=O) intermediates of cytochromes P450, the peroxidases,[8] as well as the a_3 heme of cytochrome oxidase,[9] or to oxygenate its own heme, as in heme oxygenase,[1−3] would be modulated by the electronic properties of the protein-provided heme ligand,[53] as well as the heme−polypeptide interactions that in the cases of cytochromes P450 and the peroxidases presumably retard the attack of the bound hydroperoxide on the *meso*-carbons, and accelerate the decay toward Fe^{IV}=O, and possibly prevent ruffling of the porphyrinate ring. Stabilization of the ruffled porphyrinate ring at ambient temperature positions the *meso*-carbons as much as 0.5 to 0.6 Å above or below the porphyrin mean plane,[13−16] and also places the unpaired electron of low-spin Fe(III) in the d_{xy} orbital, hence creating large spin density at the *meso*-carbons. The end result is that two of the *meso*-carbons are placed closer to the terminal OH of the Fe^{III}-OOH moiety at any given moment, thus facilitating their attack by the peroxide ligand. Whether the α- and γ- or the β- and δ-*meso*-carbons are placed closer to the terminal OH of Fe^{III}-OOH at the moment of attack is likely to be dictated by steric interactions between the porphyrin ring and the polypeptide. Moreover, since heme ruffling positions pairs of *meso*-carbons (e.g., α- and γ-) closer to the reactive Fe^{III}-OOH, if only the α-meso-carbon is attacked, as is observed in HO, this implies that the other *meso*-carbons must be sterically protected. Hence, the regioselectivity of heme oxygenation may be controlled by electronic, as well as steric, effects.

It is interesting that the model complexes used in this study suggest a dynamic equilibrium between a ruffled (d_{xy}) and a planar (d_π) conformation. Over the range of temperatures of the NMR measurements, both electronic states are present and rapidly interconverting, and at physiologically relevant temperatures the d_{xy} electron configuration is favored ($\Delta G_{310} = -1.19$ kJ/mol; $K_{eq} = 6.9$). In fact, it may be that this dynamic equilibrium, which in an enzyme may be significantly affected by heme−polypeptide interactions, is an important modulatory mechanism that helps an enzyme channel the Fe^{III}-OOH intermediate toward the formation of a ferryl intermediate in some cases, or toward heme oxygenation in others. In this context, it is interesting to point out that the crystal structures of human[54] and bacterial[55] heme oxygenase strongly suggest that the flexibility of the distal pocket, provided by conserved glycine residues 139 and 143, is an important and conserved motif in these different heme oxygenases. It is therefore tempting to speculate that the flexibility of the distal pocket in heme oxygenase functions to facilitate the dynamic equilibrium between ruffled (d_{xy}) and planar (d_π) conformers, thus channeling the reactivity of the Fe^{III}-OOH intermediate toward heme oxygenation, rather than ferryl formation. In fact, when Gly-139 of human HO-1 is mutated for a residue with a bulkier side chain, the resultant enzyme displays peroxidase-type reactivity,[56] and when similar mutations are introduced at position 143, the mutant enzymes lose their oxygen activation activity.[57]

Another important modulatory mechanism among the enzymes that react through the Fe^{III}-OOH intermediate is that provided by the proximal heme ligand, a histidine in the cases of heme oxygenase, the peroxidases, and cytochrome *c* oxidase, but a cysteinate in the cases of the cytochromes P450 and chloroperoxidase. It is thus possible that in addition to the dynamic equilibrium discussed above, an additional modulatory mechanism among the enzymes that react through the Fe^{III}-OOH intermediate is provided by the chemical nature of the proximal ligand, including the histidine imidazole protonation state. For example, it is thought that in cytochrome P450, the proximal cysteinate ligand destabilizes the O−O bond through strong electron donation, in conjunction with electron withdrawal from a hydrogen bond network in the distal site of the heme binding domain.[58] In peroxidases the same "push−pull" mechanism is thought to be operative because the proximal His ligand is ionized or strongly hydrogen bonded.[58] It has been previously proposed that in HO, the lack of effectiveness of the neutral His ligand as an electron donor may actually lower the rate of O−O cleavage, hence channeling the reaction toward heme oxygenation rather than ferryl complex formation.[10,59] It is therefore important to investigate the effect that the protonation state of the proximal ligand might have on the dynamic equilibrium between planar (d_π) and ruffled (d_{xy}) conformers, and such studies are in progress in our laboratories.

If the $Fe^{III}(por^{2-})(^{-}OOH)$ complex in HO indeed has the unpaired electron in the d_{xy} orbital, then large spin density is expected to be present at the *meso*-carbons due to partial porphyrin-to-metal electron transfer.[13−16] A limiting resonance structure for such a species is that in which the electron is fully transferred from the porphyrinate ring to the metal, and may be represented as $Fe^{II}(por^{-\bullet})(^{-}OOH)$, which raises the possibility of involvement of a radical mechanism for this enzyme. A radical mechanism was considered previously, but discarded because the then proposed radical (•OH) was thought to be too indiscriminate to lead to well-controlled reactivity.[10] However, if the limiting structure $Fe^{II}(por^{-\bullet})(OOH)$ is considered, then attack of •OH at a *meso*-carbon would produce Fe^{II}(por-*meso*-H,OH)($O^{-\bullet}$), which would rapidly rearrange its Fe−O electron configuration, lose the proton from the attacked meso position to re-aromatize the porphyrin ring, and reprotonate the Fe^{III}-O^{2-} to yield the resting Fe^{III} aquo form of the enzyme. It is therefore evident that if the Fe^{III}-OOH intermediate of heme oxygenase does indeed have its unpaired electron residing in the d_{xy} orbital, the electronic structure of the intermediate, which, as we have shown with the model ferriheme complexes, is accessible via a dynamic equilibrium that is influenced by the proximal ligand and the surrounding polypeptide, becomes a novel mechanism by which this obligatory intermediate is channeled to favor either heme oxygenation or monooxygenation activity.

It is also noteworthy that bis-pyridine complexes of model *meso*-hydroxyhemes such as OEPO, produced by coupled oxidation of OEPFe(III),[14,16,60−62] have more compressed EPR

(53) This certainly includes hydrogen-bonding/deprotonation of histidine ligands of the peroxidases as compared to HO.
(54) Schuller, D. J.; Wilks, A.; Ortiz de Montellano, P. R.; Poulos, T. L. *Nat. Struct. Biol.* **1999**, *6*, 860−867.
(55) Schuller, D. J.; Zhu, W.; Stojiljkovic, I.; Wilks, A.; Poulos, T. L. *Biochemistry* **2001**, *40*, 11552−11558.
(56) Liu, Y.; Koenigs Lightning, L.; Huang, H.; Moënne-Loccoz, P.; Schuller, D. J.; Poulos, T. L.; Loehr, T. M.; Ortiz de Montellano, P. R. *J. Biol. Chem.* **2000**, *275*, 34501−34507.
(57) Koenigs Lightning, L.; Huang, H.; Moënne-Loccoz, P.; Loehr, T. M.; Schuller, D. J.; Poulos, T. L.; Ortiz de Montellano, P. R. *J. Biol. Chem.* **2001**, *276*, 10612−10619.
(58) Marnett, L. J.; Kennedy, T. A. In *Cytochrome P450: Structure, Mechanism, and Biochemistry*, 2nd ed.; Ortiz de Montellano, P. R., Ed.; Plenum Press: New York, 1995; pp 49−80.
(59) Wilks, A.; Ortiz de Montellano, P. R. *J. Biol. Chem.* **1993**, *268*, 22357−22362.
(60) Balch, A. L.; Latos-Grażyński, L.; Noll, B. C.; Szterenberg, L.; Zovinka, E. P. *J. Am. Chem. Soc.* **1993**, *115*, 11846−11854.

spectra than do their OEPFe(III) counterparts. These observations suggest that that *meso*-hydroxyheme complexes may favor the d_{xy} electron configuration and its limiting Fe^{II}(OEPO) radical resonance structure, and thus facilitate the next step in the HO reaction, again by a radical mechanism. Magnetic resonance and chemical reactivity investigations of the alkylperoxide and hydroperoxide complexes of model *meso*-hydroxyhemes and several heme proteins are in progress in our laboratories.

(61) Balch, A. L.; Latos-Grażyński, L.; St. Claire, T. N. *Inorg. Chem.* **1995**, *34*, 1395−1401.
(62) Balch, A. L.; Koerner, R.; Latos-Grażyński, L.; Noll, B. C. *J. Am. Chem. Soc.* **1996**, *118*, 2760−2761.

Acknowledgment. This work was supported by NIH grants GM-50503 (M.R.), DK-31038 (F.A.W.), OCAST grant HR00-043 (M.R.), and by NSF grant DBI-9604939 for pulsed ENDOR instrument construction (A.M.R., F.A.W.).

Supporting Information Available: Figure S1, pulsed ENDOR spectra of $[TPPFe(OCH_3)_2]^-$ and $[TPPFe(OO^tBu)_2]^-$; Figure S2, temperature dependence of the *meso*-^{13}C signals of $[TPPFe(OCH_3)(OO^tBu)]^-$ and $[TPPFe(OO^tBu)_2]^-$ (PDF). This material is available free of charge via the Internet at http://pubs.acs.org.

JA017334O